Phonons in liquid ^{4}He from a heated metal film. II. The angular distribution

1994 J. Phys.: Condens. Matter 6 2825

(http://iopscience.iop.org/0953-8984/6/15/005)

J. Phys.: Condens. Matter 6 (1994) 2825–2834. Printed in the UK

Phonons in liquid ^{4}He from a heated metal film: II. The angular distribution

M A H Tucker and A F G Wyatt
Department of Physics, University of Exeter, Stocker Road, Exeter EX4 4QL, UK

Received 15 December 1993, in final form 27 January 1994

Abstract. We have measured the angular distribution of phonons emitted by an Au film heater in liquid ^{4}He. For long heater pulses (10 μs), the distribution is almost Lambertian ($\propto \cos\theta$), but for short pulses (0.1 μs), the distribution is very anisotropic. The HWHM of the beam of high-frequency ($\hbar\omega/k_B > 10$ K) phonons is $\sim 3.5°$, and the HWHM of the low-frequency ($\hbar\omega/k_B < 1$ K) phonon beam is $\sim 10.5°$. We suggest that the angular distribution of the low-frequency phonons is due initially to classical phonon transmission at the heater/^{4}He interface, but is then broadened by decays and interactions in the liquid. These interactions in the liquid create the high-frequency phonons. The high-frequency phonon beam is narrower than the low-frequency phonon beam due to momentum conservation in the four-phonon process (4PP) interactions that create them. Narrow beams of phonon emission from cleaved crystal surfaces have been observed before, but we believe that this is the first time that similarly narrow beams from evaporated metal surfaces have been observed.

1. Introduction

The existence of a finite discontinuity in temperature at an interface between two materials has led to several models of how this thermal boundary resistance arises. In the case of two solids in contact, the acoustic mismatch model (AMM) [1] together with a contribution from diffuse phonon scattering due to the interfacial disorder gives reasonable agreement with measurements [2–6]. For a boundary between liquid ^{4}He and a solid, with which we are concerned in this paper, the energy transmission through the interface (Kapitza conductance) is also a mixture of the AMM [7] and other channels [8–10]. These additional channels dominate the Kapitza conductance. The minor role of the AMM in the thermal conductivity across an interface between a solid and liquid ^{4}He is due to the large mismatch in acoustic impedance. The importance of the additional channels relative to the AMM is a strong function of the quality of the solid surface [11], especially when the surface is nearly perfect [12].

In the AMM [7], a single phonon in material 1 is transmitted, with probability α, through the interface into material 2. Energy and momentum parallel to the interface are conserved, which constrains the phonons in the material with the smaller phonon velocities into a narrow cone. This is called the elastic channel, and the thermal conductivities have been calculated [7, 13]. In the inelastic channel, a single phonon is absorbed at the surface and the energy (one or more phonons) is then re-radiated according to the momentum space available either side of the interface. (If more than one phonon is radiated, the phonon frequencies are down converted.) This has been called the diffuse mismatch model [10]. Energy, but not parallel momentum, is conserved between the incoming and outgoing phonons, and the emission is consequently more isotropic than in the AMM. Theoretical studies show that the

0953-8984/94/152825+10$19.50

inelastic channel is negligible compared with the elastic channel if the interface is perfectly flat, so surface scattering centres had to be invoked to account for the measured Kapitza conductance [14].

The measured Kapitza conductance for a liquid ^{4}He/solid interface is greater than the prediction of the AMM due to the inelastic channel, but tends towards the AMM value at low temperatures [15]. In the AMM, the transmission probability for phonons through the interface is independent of phonon frequency ω. The temperature dependence of the Kapitza conductance has been used to obtain a description of $\alpha(\omega)$, the transmission probability summed over all possible channels [8, 16].

We now briefly summarize the experimental evidence for the emission cones of the AMM for, firstly, dielectric crystals and, secondly, metals.

Transmission via both AMM and inelastic channels has been observed to take place across very flat, clean interfaces between dielectric crystals and liquid ^{4}He [11, 12, 17]. The angular distribution of phonons emitted from a cleaved crystal surface into liquid ^{4}He shows a high intensity in a narrow cone of angles perpendicular to the crystal surface, superimposed upon a $\cos\theta$ component ($\theta = 0$ in the direction of the surface normal) [17]. The angular width and detailed shape of the cone are in good agreement with the AMM of phonon transmission across a solid/^{4}He interface [9, 17]. The cone width is determined by the ratio of phonon velocities in the two materials in contact and the conservation of momentum parallel to the interface. Slight contamination of the cleaved crystal surface results in a deterioration in the intensity of the narrow cone, and an increase in the isotropic background [9]. By using a superconducting tunnel junction (STJ) detector with an energy threshold of $2\Delta/k_B = 4.2$ K, it was shown that the spectrum of phonons emitted into the narrow cone has a higher effective temperature than those in the $\cos\theta$ background [18]. The $\cos\theta$ background of low-frequency phonons was therefore identified with the inelastic channel processes, where more than one phonon in the liquid is produced by one phonon in the solid. It has been found that only 0.02 atomic layers of impurities condensed onto a previously annealed crystal surface are necessary for the inelastic channel of energy transmission to become significant [12].

For a metal film evaporated onto a glass substrate, the exposed metal surface is expected to be uneven on the scale of thermal phonon wavelengths. Electron micrographs of various Au film heaters used in our experiments exhibit some surface unevenness at length scales of < 1 μm as shown in figure 1. Some heaters show a mainly undulating surface whereas other heaters appear to have an almost completely flat surface down to length scales of < 0.1 μm. The heater used in the experiment described in this paper is one that had little surface unevenness discernible in the micrograph (figure 1(*b*)). Assuming that the AMM of emission applies to each crystalline facet on the heater surface, the random orientation of the facets should result in a broadening of the angular emission [19]. Also, the presence of grain boundaries would favour the broad background of low-frequency phonons emitted via the inelastic channel [20]. The angular distribution of phonon signals from film heaters has previously been measured, but only for long heater pulses $t_p \geqslant 5$ μs. No sharp emission cones readily identifiable with the AMM have been observed with metal surfaces in liquid ^{4}He.

For $t_p = 300$ μs, the phonon distribution emitted from C film heaters at low powers (< 4 mW mm^{-2}) was measured to be proportional to $\cos\theta$ (Lambertian) [21]. At higher heater powers (> 8 mW mm^{-2}), the emission became more isotropic, corresponding to a hemispherical heat source. Similar angular distributions of emission were observed with films with different surface structure.

For $t_p = 5$ μs, it was observed that the angular distribution of phonon signals from

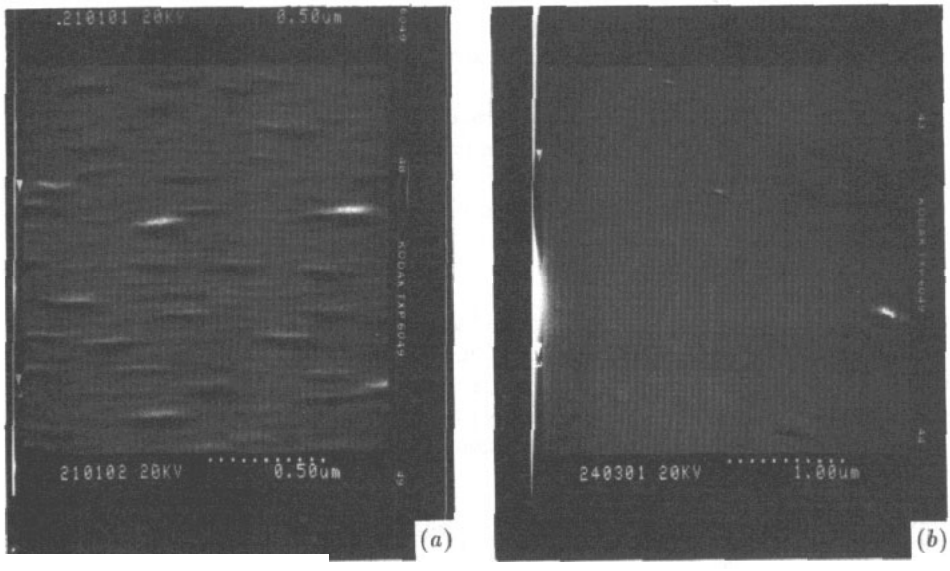

Figure 1. Electron micrographs of the surfaces of two Au film heaters. The incident electron beam is at 80° to the heater normal. (*a*) A film with evident surface roughness, which was used for some of the data presented in part I of this double paper [24]. The horizontal field of view is 1.5 μm. (*b*) A film with little discernible surface unevenness, which was used for the angular distribution data presented in this paper. The horizontal field of view is 3.0 μm.

an Au film heater was slightly narrower than Lambertian, and could be parameterized by $\cos^n\theta$, where $1 < n < 2$ [22].

For $t_p = 1$ μs, another experiment has indicated an even greater deviation from Lambertian emission [23]. A constantan heater was pulsed for 1 μs at various powers, and the phonons were detected by an STJ. The results could only be accounted for if the angular distribution of these $\hbar\omega > 2\Delta$ phonons was strongly peaked in the forward direction. At a power of 5 mW mm^{-2}, the signal at $\theta = 0°$ (normal to the heater plane) was ~ 18 times that expected from Lambertian emission. It was estimated that most of the phonons were emitted into $\theta < 30°$, and a parameterization of $\cos^{21}\theta$ was suggested. Taken together, these experimental results suggest that as the heater pulse length is decreased, the phonon emission from a heater into liquid ^{4}He exhibits greater anisotropy.

We have previously shown that for very short pulse lengths ($t_p < 0.25$ μs) and medium heater powers (2–40 mW mm^{-2}), the high-frequency phonon signal is clearly observable in $\theta = 0°$ signals [24]. We will now show that it is in fact much larger than would be expected for Lambertian emission. This excess of high-frequency phonons in $\theta = 0°$ signals has been observed in all Au, Cr, and non-superconducting Ti film heaters [25] that we have investigated so far.

Let S_H and S_L be the signals at $\theta = 0$ integrated over time for high- and low-frequency phonons respectively. Then

$$\frac{S_H}{S_L} = \int_{\omega_c}^{\omega_{max}} G(\omega)\alpha(\omega)E(\omega)\,d\omega \Big/ \int_0^{\omega_c} G(\omega)\alpha(\omega)E(\omega)\,d\omega \tag{1}$$

where $G(\omega)$ is the geometric factor, $\alpha(\omega)$ is the transmission probability into the bolometer at normal incidence, and $E(\omega)$ is the phonon energy distribution created in the liquid He

by the heater. The geometric factor $G(\omega)$ is a measure of the angular emission of phonons from the heater. The limits of the integrals are $\hbar\omega_c/k_B = 10$ K, the threshold of stability for high-frequency phonons, and ω_{max}, the maximum phonon frequency, which occurs at the maxon.

The qualitative form of $\alpha(\omega)$ has been derived from temperature dependences of the Kapitza conductance, and one such approximation is [16]

$$\alpha(\hbar\omega < 5k_B) = \alpha_{AMM} + (\hbar\omega/5k_B)(\alpha_0 - \alpha_{AMM}) \tag{2a}$$

$$\alpha(\hbar\omega > 5k_B) = \alpha_0 \tag{2b}$$

where α_{AMM} is the acoustic mismatch value. For phonons crossing the interface from a solid to the liquid ^{4}He, $\alpha_{AMM} = 7 \times 10^{-3}$ for Zn, and $\alpha_0 = 0.5$. For phonons crossing the interface from the liquid ^{4}He to the solid, these transmission coefficients are modified by a factor that cancels out in the following analysis. Because both low- and high-frequency phonon distributions have narrow spectral widths [24], then assuming that $G(\omega)$ does not vary rapidly within either frequency range,

$$\frac{S_H}{S_L} \simeq \left(\frac{G_H}{G_L}\right) \frac{\alpha_0}{[\alpha_{AMM} + (\hbar\bar{\omega}/5k_B)(\alpha_0 - \alpha_{AMM})]} \int_{\omega_c}^{\omega_{max}} E(\omega)\,d\omega \Big/ \int_0^{\omega_c} E(\omega)\,d\omega \tag{3}$$

where $\hbar\bar{\omega}$ is the average energy of the low-frequency phonons reaching the bolometer, and G_H and G_L are mean geometric factors for high- and low-frequency phonons respectively. Using $\hbar\bar{\omega}/k_B = 0.5$ K due to spontaneous decays

$$\frac{S_H}{S_L} \simeq 9\left(\frac{G_H}{G_L}\right) \int_{\omega_c}^{\omega_{max}} E(\omega)\,d\omega \Big/ \int_0^{\omega_c} E(\omega)\,d\omega \simeq 5 \times 10^{-2}\left(\frac{G_H}{G_L}\right). \tag{4}$$

We have assumed that the partition of energy between $\omega > \omega_c$ and $\omega < \omega_c$ phonons has the ratio of 5.5×10^{-3}. This has been estimated using two Planck distributions with $T_p = 0.7$ K (background channel) and $T_p = 1.9$ K (elastic channel) [19].

So, if both the high- and low-frequency phonons are emitted from the heater with the same angular distribution, then the signal due to high-frequency phonons should be about 20 times smaller than the signal due to low-frequency phonons. However, the observed value of $S_H/S_L = 2.5$ implies that the ratio of geometric factors for high- and low-frequency phonons is $G_H/G_L \simeq 50$. If the high- and low-frequency phonons are emitted into cones of half angle θ_H and θ_L respectively, then

$$G_H/G_L \simeq (1 - \cos\theta_L)/(1 - \cos\theta_H). \tag{5}$$

This requires $\theta_H < 11.5°$ if $\theta_L < 90°$ which inspired us to measure the angular distributions of phonons emitted from these metal film heaters.

2. Experiment

The experimental cell was cooled to $\sim$ 60 mK by a dilution refrigerator, and the cell was filled with purified liquid ^{4}He [26]. Inside the cell are two heaters, two bolometers, a superconducting stepper motor, and a calibrated RuO chip thermometer. A schematic diagram is shown in figure 2. Each heater is a 1 mm^2 Au film of $R \simeq 50\ \Omega$, evaporated

onto a glass substrate. The 1 mm^2 Zn film bolometers are operated on their superconducting transitions. The main heater and bolometer pair face each other at a separation of 15.6 ± 0.1 mm. The main heater is mounted on an axle that is tilted using the geared down stepper motor. An arm connects this axle to a second heater, which faces the secondary bolometer. The separation between the secondary heater/bolometer pair is measured using the time of flight of low-frequency phonons, which travel at 238 m s^{-1}. This separation gives the angle of tilt θ of the main heater, which is the angle between the normal to the heater plane and the geometric line connecting the centres of the heater and bolometer. No collimation was present. The data acquisition system is outlined in [24].

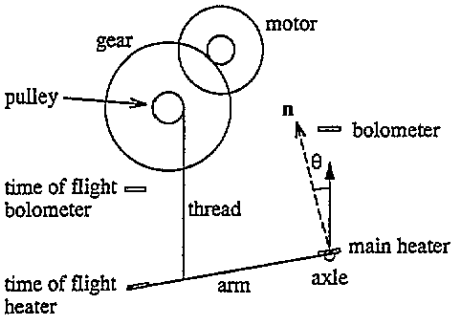

Figure 2. A schematic diagram of the apparatus. The motor was geared down to reduce the size of the steps in θ. The angle of tilt θ was calculated from the time of flight of low-frequency phonons, which travel at the ultrasonic velocity, between the heater and bolometer on the left.

3. Results

Phonon signals were measured at various tilt angles θ of the heater. A pulse of $t_p = 0.1$ μs, power= 10 mW mm^{-2} was used to study both the high- and low-frequency phonons. For comparison with previously published data, a pulse of 10 μs duration and 1 mW mm^{-2} power was also used to study low-frequency phonons only. We use a lower power for the long pulse length for two reasons. Firstly, this power is below the soft threshold ($\sim$ 2 mW mm^{-2}) for the creation of a detectable number of high-frequency phonons. Secondly, reducing the power should decrease any effect that interactions between injected phonons might have on any initial angular anisotropy. Using these two pulse lengths gives us information on how important t_p is to the angular emission.

We present first the angular scan of the 10 μs pulses because this links in with published results from previous experiments. The signal at $\theta = 3.5°$ is shown in figure 3. We believe that the long tail is due to phonon emission from the cooling substrate beneath the metal film of the heater, so we exclude this tail from the integration of the signal over time by integrating from t_1 to t_2. The integrated signal as a function of angle is almost Lambertian, as shown in figure 5.

The results from the very short (0.1 μs) pulses are markedly different, as shown in figure 4. Both the low-frequency and high-frequency phonon peaks decrease rapidly as the angle θ increases from 0°. The integrated signals as a function of angle θ are shown in figure 5. The long tail from the first peak in the signal is excluded from the integrations of both the low- and high-frequency phonon signals.

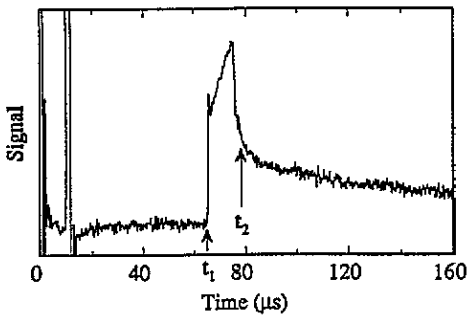

Figure 3. The signal detected from a 10 μs, 1 mW mm^{-2} heater pulse at $\theta = 3.5°$. The signal tail ($t > t_2$) is most likely to be due to the emission of phonons by the heater substrate.

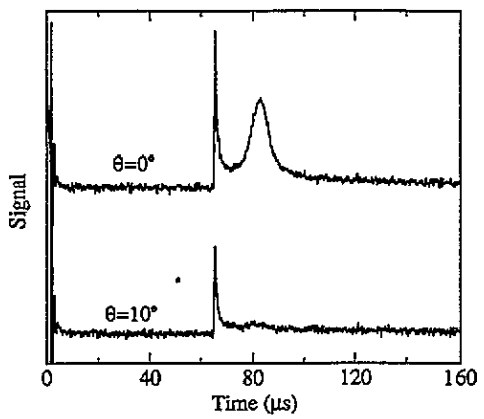

Figure 4. Signals from 0.1 μs, 10 mW mm^{-2} heater pulses observed at $\theta = 0°$ and 10° at SVP. The path length is 15.6 ± 0.1 mm; $T < 0.1$ K.

The intensity of high-frequency phonons is immeasurably small for $\theta > 12°$, whereas the intensity of low-frequency phonons is measurable at all angles. For $\theta > 30°$, there are indications that the low-frequency phonon emission is almost Lambertian. So at small angles, there is probably a narrow cone of low-frequency phonons superimposed upon a $\cos\theta$ background of low-frequency phonons. The angular width of the low-frequency phonon beam, the half width at half maximum (HWHM), is approximately 10.5° after the $\cos\theta$ background has been subtracted. The measurement of the angular distribution of low-frequency phonons is hardly affected by the finite size of the bolometer, which subtends an angular width of $\sim 3.5°$. The measured HWHM of the high-frequency phonon beam is about 4°. When the finite sizes of the heater and bolometer are taken into account, this gives a deconvolved HWHM of $\sim 3.5°$ for a point source of high-frequency phonons on the heater surface.

These narrow angles of $\sim 3.5°$ and $\sim 10.5°$ are extremely surprising for an uncollimated signal from a heated metal film, and therefore require a thorough explanation. Much of the groundwork for the following discussion was laid out in part I of this double paper [24].

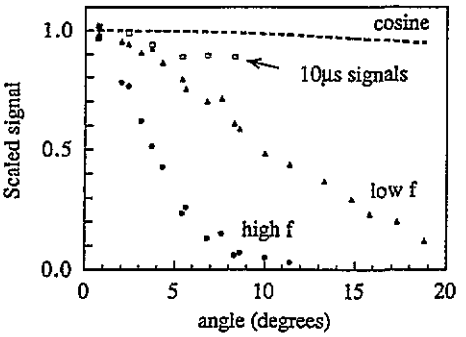

Figure 5. The angular dependences of low-frequency (low f) and high frequency (high f) phonon signals from an Au heater for 0.1 μs, 10 mW mm^{-2}. A $\cos\theta$ distribution fitted to the large-angle ($\theta > 30°$) data has been subtracted from the 'low f' data. Also shown are the integrated signals (t_1–t_2) from 10 μs, 1 mW mm^{-2} heater pulses, and the Lambertian ($\cos\theta$) distribution. All are scaled to be equal at $\theta = 0°$.

4. Discussion

These results provide an explanation for the observed angular dependences of phonon–atom evaporation signals [27]. The quantum evaporation signals occurred at the correct angle, but the angular width of the desorbed atom beam was less than the calculated value. This can now be seen as due to the narrow beam of almost monoenergetic high-frequency phonons created by the heater.

The only model that can currently be used to explain the anisotropic emission of phonons observed at short pulse lengths is the AMM. From the conservation of momentum parallel to the interface as energy is transferred from a phonon in the heater to a phonon in the liquid, the maximum angle θ_c of this emitted phonon to the normal is given by $\sin\theta_c = c_L/c_S$, where c_L and c_S are the phonon velocities in the liquid and solid respectively. Because there are two polarizations of phonons in the solid, longitudinal l and transverse t, but only longitudinal phonons exist in the liquid, there are two cone angles, which for Au are $\theta_C^{(l)} = 4.25°$ and $\theta_C^{(t)} = 11.4°$.

The first, and perhaps the most obvious, observation is that these critical angles correspond remarkably well with the HWHM of the high- and low-frequency phonon beams in figure 5. Perhaps then, in such a case, the critical angles of the acoustic mismatch cones from each orientation of crystalline facets on the almost flat surface are softened into the HWHM of the signal profile from the whole heater surface. However, to tie in with the phonon frequency distributions, this scenario would require that longitudinal phonons in the heater would have to preferentially transfer their energy to single phonons in the liquid, whereas transverse phonons would have to preferentially emit two or more low-frequency phonons into the liquid to give the energy down conversion, with some conservation of momentum parallel to the surface to give the observed phonon beam (on the assumption that the transverse and longitudinal phonon distributions in the heater have the same effective temperature). This effect has not been seen to occur at crystal surfaces, where the emission cone is due to all the phonon polarizations in the crystal [17], and down conversion gives a $\cos\theta$ distribution [18,9].

Moreover, we have deduced from the shape of the spectrum of detected high-frequency phonons that they are created in the liquid by interactions between lower-frequency injected phonons [24]. If the low-frequency phonon injection is anisotropic, then the high-frequency

phonon creation will be also. Consider two phonons of similar energy ($\hbar\omega/k_B \simeq 5.5$ K) at angles θ_1 and θ_2 to the normal and with randomly selected azimuthal angles ϕ_1 and ϕ_2, combining to create a third phonon of nearly twice the energy at an angle of θ_3 to the normal, together with another phonon that has little energy (figure 6). A four-phonon interaction (4PP) at least is necessary to create these high-frequency phonons because of the 3PP cut-off at $\sim$ 8 K. If the fourth phonon is indeed of low energy, then θ_3 is less than the larger of θ_1 and θ_2 in the majority of cases, and so the high-frequency phonons have a narrower angular distribution than the low-frequency phonons. So, we should compare the angular distribution of only the low-frequency phonons with the AMM.

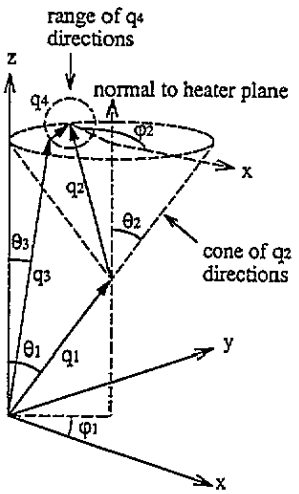

Figure 6. An illustrative vector diagram of a four-phonon interaction showing that if the momentum (q_4) of one of the outgoing phonons is much less than the momenta (q_1 and q_2) of both the incoming phonons, then the angle θ_3 of the high-frequency outgoing phonon to the heater normal is less than the larger of θ_1 and θ_2, the angles of the incoming phonons to the heater normal, in the majority of cases. So a four-phonon interaction can give rise to an angular distribution of high-frequency phonons narrower than that of the injected lower-frequency phonons.

The injected low-frequency phonon beam could actually be narrower than the measurements shown in figure 5 suggest for two main reasons. Firstly, spontaneous phonon decays will take place at all distances from the heater. Although the opening angles in these spontaneous decays are small for each decay (a few degrees), the final phonons can be travelling in a direction deviated over as much as 20° from the initial phonon direction due to successive decays as the phonons cascade down to low frequencies. Secondly, the fourth phonon from the 4PP will have a fairly wide range of angles (figure 6) and so during the interactions that create the high-frequency beam, the low-frequency phonon beam broadens. So, it appears that for very short pulse lengths, a large fraction of the low-frequency phonons are injected into the liquid within the angles determined by the AMM cone.

We know that for $t_p < 0.25$ μs at heater powers around 10 mW mm^{-2}, the high-frequency phonons are created by interactions between lower-frequency phonons, and that at greater pulse lengths, no further detectable high-frequency phonons are produced [24]. It appears that for $t_p > 0.25$ μs, additional scattering processes in front of the heater disrupt

further high-frequency phonon production [28]. It is probable that these extra processes broaden the low-frequency phonon beam, and due to this broadening, the angular correlation required to create the high-frequency phonons is largely lost (see figure 6).

In contrast to these results for a metal film, no significant broadening of phonon beams beyond the acoustic mismatch critical angles has been reported for clean dielectric crystal surfaces even though long (5 μs) pulses were used [17]. One possibility for this difference is that the phonon transmission probabilities at the crystal surfaces reduces the energy flux in the He from the heater. Other possibilities are that (i) any slight roughness of the metal surface introduces the randomization of angles needed to seed the interactions, whereas a crystal surface is too flat, and (ii) the conduction electrons in the metal affect the phonons in the liquid [29, 13].

5. Summary

We have measured the angular distribution of phonons emitted by an Au film heater into liquid ^{4}He. For long pulses, the distribution is almost Lambertian, but for short heater pulses, the distribution is very anisotropic. The HWHM of the high-frequency phonon beam is $\sim 3.5°$, and the HWHM of the low-frequency phonon beam is $\sim 10.5°$. We have previously shown that the high-frequency phonons are created in the liquid by interactions between low-frequency phonons. We suggest that the angular distribution of the low-frequency phonons is due initially to classical phonon transmission, but is then broadened by decays and interactions in the liquid. We also suggest that the AMM can therefore only be investigated experimentally with metals when using a heat pulse technique with sufficiently short pulses ($t_p < 0.25$ μs), and at lower powers ($W < 1$ mW mm^{-2}) to reduce the effect of phonon interactions. Repeating this experiment at higher pressures should reveal whether the narrow phonon beams are shepherded by the critical angles of the AMM, because phonon velocities in liquid ^{4}He change quite rapidly with pressure. Also, phonon decays are eliminated for $P > 19$ bar [30].

In conclusion, we have discovered that if the parameters of a heater pulse are correctly chosen, we obtain a narrow beam of almost monoenergetic high-frequency phonons. This beam should be of some use in probing various processes in the bulk liquid and at its boundaries.

Acknowledgments

This work was made possible by a SERC/NATO postdoctoral research fellowship. We thank the University of Exeter for the use of its resources, and especially Mr C Lovell for the electron micrographs.

References

[1] Little W A 1959 *Can. J. Phys.* **37** 334–9
[2] Herth P and Weis O 1970 *Z. Angew. Phys.* **29** 101–6
[3] Weis O 1972 *J. Physique Coll.* **33** C4 49–56
[4] Cheeke J D N, Herbral B and Martinon C 1972 *J. Physique Coll.* **33** C4 57–9
[5] Anderson A C 1981 *Nonequilibrium Superconductivity, Phonons and Kapitza Boundaries* (New York: Plenum) ch 1

[6] Kechrachos D 1991 *J. Phys.: Condens. Matter* **3** 1443–52
[7] Khalatnikov I M 1965 *An Introduction to the Theory of Superfluidity* (New York: Benjamin)
[8] Challis L J 1974 *J. Phys. C: Solid State Phys.* **3** 481–95
[9] Wyatt A F G 1981 *Nonequilibrium Superconductivity, Phonons and Kapitza Boundaries* (New York: Plenum) ch 2
[10] Swartz E T and Pohl R O 1989 *Rev. Mod. Phys.* **61** 605–59
[11] Mok E, Burger S, Dottinger S, Lassmann K and Eisenmenger W 1986 *Phys. Lett.* **114A** 473–6
[12] Basso H C, Dietsche W, and Kinder H 1986 *J. Low Temp. Phys.* **65** 247–59
[13] Challis L J and Cheeke J D N 1968 *Proc. R. Soc.* A **304** 479–86
[14] Sluckin T J, Sheard F W, Bowley R M and Toombs G A 1975 *J. Phys. C: Solid State Phys.* **8** 3521–30
[15] Folinsbee J T and Anderson A C 1973 *Phys. Rev. Lett.* **31** 1580–1
[16] Bradshaw T and Wyatt A F G 1983 *J. Phys. C: Solid State Phys.* **16** 651–64
[17] Sherlock R A, Mills N G and Wyatt A F G 1975 *J. Phys. C: Solid State Phys.* **8** 300–15
[18] Wyatt A F G and Crisp G N 1978 *J. Physique Coll.* **39** C6 244–5
[19] Wyatt A F G, Lockerbie N A and Sherlock R A 1989 *J. Phys.: Condens. Matter* **1** 3507–22
[20] Haug R, Sigmund E and Weiss K 1987 *J. Low Temp. Phys.* **67** 27–46
[21] Pfeifer C D and Luszczynski K 1973 *Phys. Rev.* A **7** 1055–61
[22] Mills N G, Wyatt A F G and Sherlock R A 1975 *J. Phys. C: Solid State Phys.* **8** 289–99
[23] Lockerbie N A 1975 *PhD Thesis* University of Nottingham
[24] Tucker M A H and Wyatt A F G 1994 *J. Phys.: Condens. Matter* **6** 2813–24
[25] Chrome and titanium films supplied by Dr N Mulders
[26] Supplied by Lancaster University
[27] Brown M and Wyatt A F G 1990 *J. Phys.: Condens. Matter* **2** 5025–46
[28] Tucker M A H and Wyatt A F G *Proc. 20th Int. Conf. on Low Temperature Physics, Oregon, 1993* at press
[29] Johnson R C and Little W A 1963 *Phys. Rev.* **130** 596–604
[30] Dynes R C and Narayanamurti V 1975 *Phys. Rev.* B **12** 1720–9